Supplementary Figures and Tables

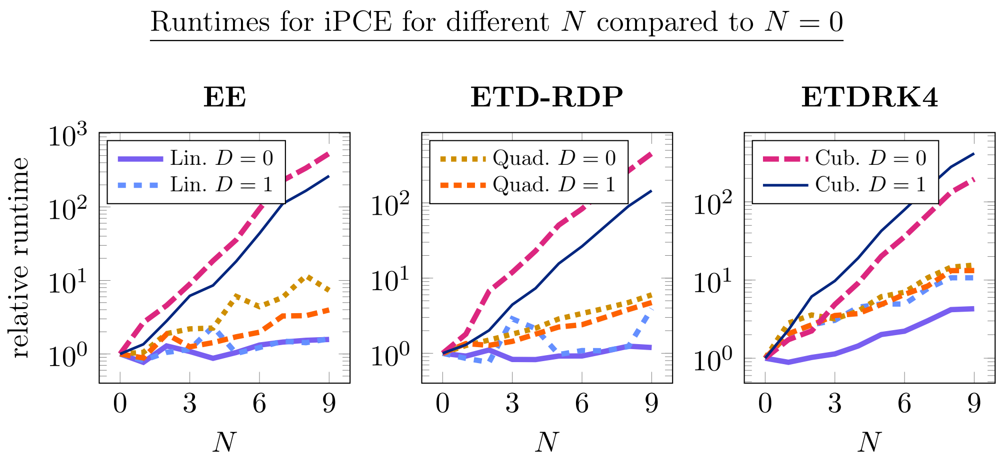

Figure 1.: Relative runtimes R_N for $N = 0, \ldots, 9$, where $R_0 := 1$. Each plot shows six curves for six different equations investigated in Section 4.1: Equation (27) with linear, quadratic or cubic F, with $D = 0$ or $D = 1$. Each data point is an average over the runtimes of ten identical iPCE simulations with $T = 0.1$ and $M = 10$ time steps. It is observed that the effort grows most slowly for linear F and most quickly (exoponentially) for cubic F.

N	0	1	2	3	4	5	6	7	8
$\tilde{N}$	1	8	39	124	335	762	1589	3016	5418

Table 1.: Number $\tilde{N}$ of summands in equation (20) for low N. Of these, $\tilde{N}/(N+1)$ are nonzero.

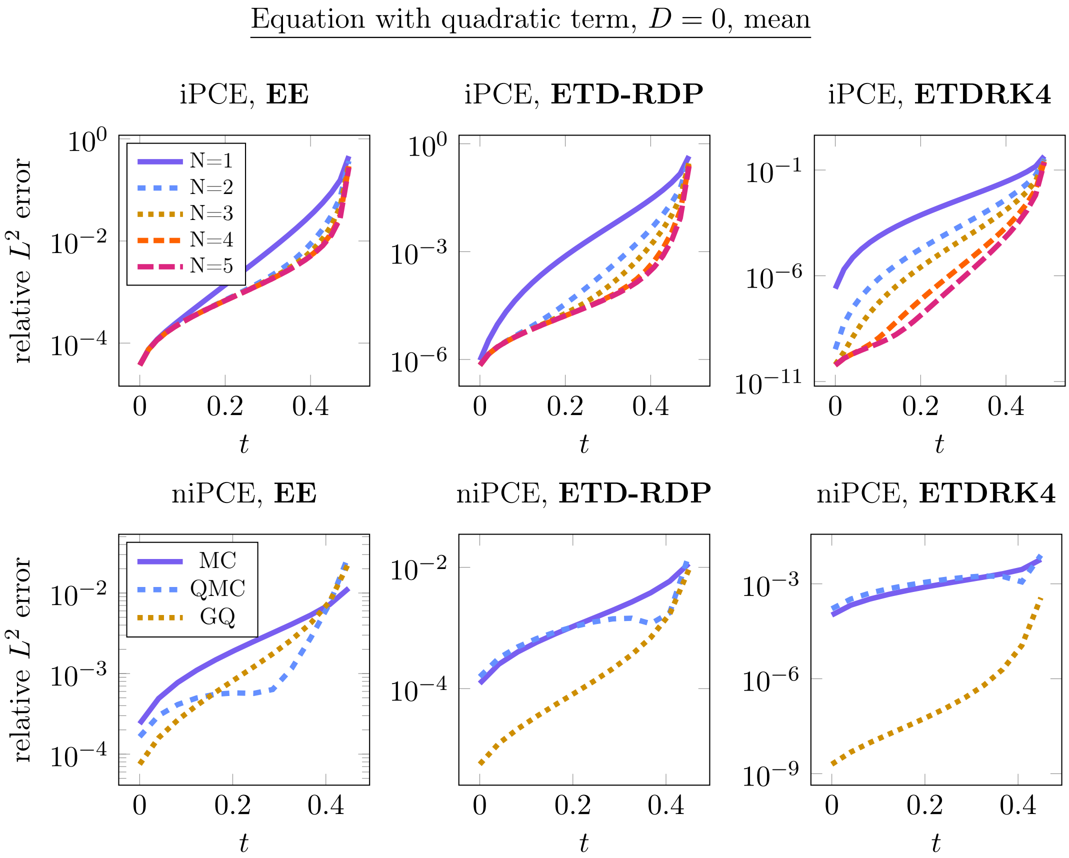

Figure 2.: Plots showing the relative time-dependent error for iPCE schemes (Algorithms 3.5, 3.6, 3.8; left-hand side) and niPCE schemes (right-hand side) for equation (26) with quadratic term ($\kappa = 2$) with diffusion constant $D = 0$.

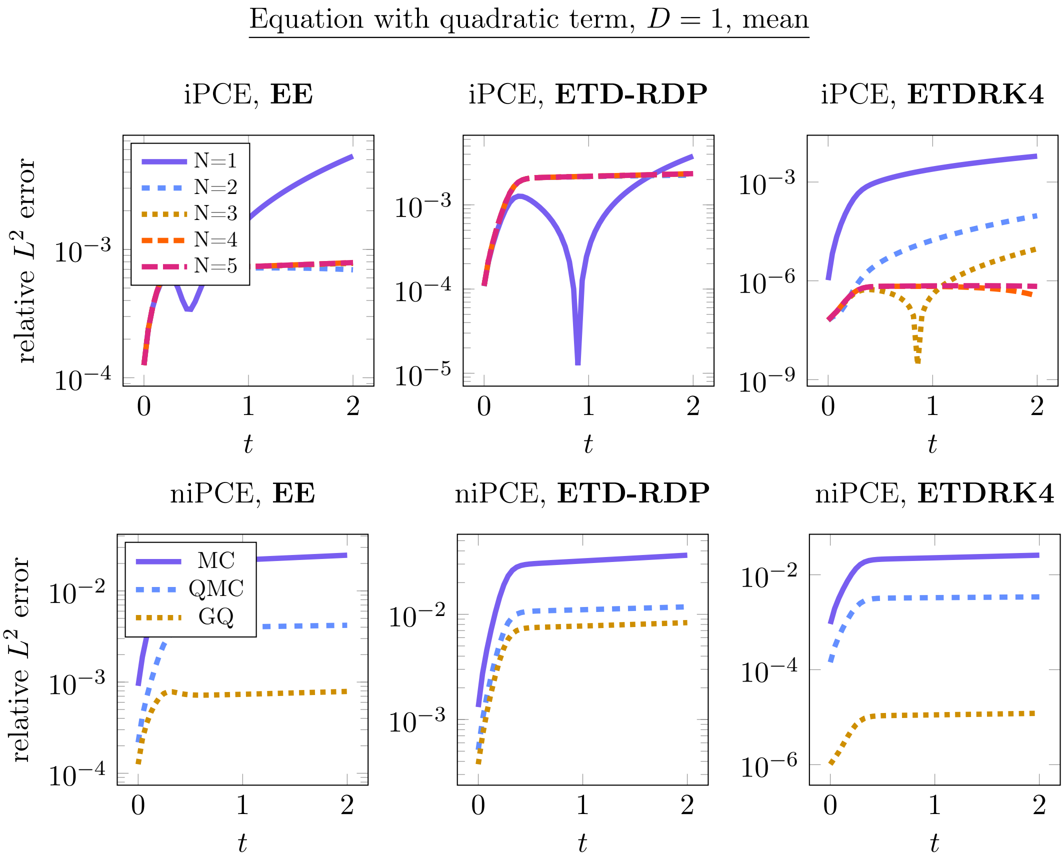

Figure 3.: Plots showing the relative time-dependent error for iPCE schemes (Algorithms 3.5, 3.6, 3.8;, left-hand side) and niPCE schemes (right-hand side) for equation (26) with quadratic term ($\kappa = 2$) with diffusion constant $D = 1$.

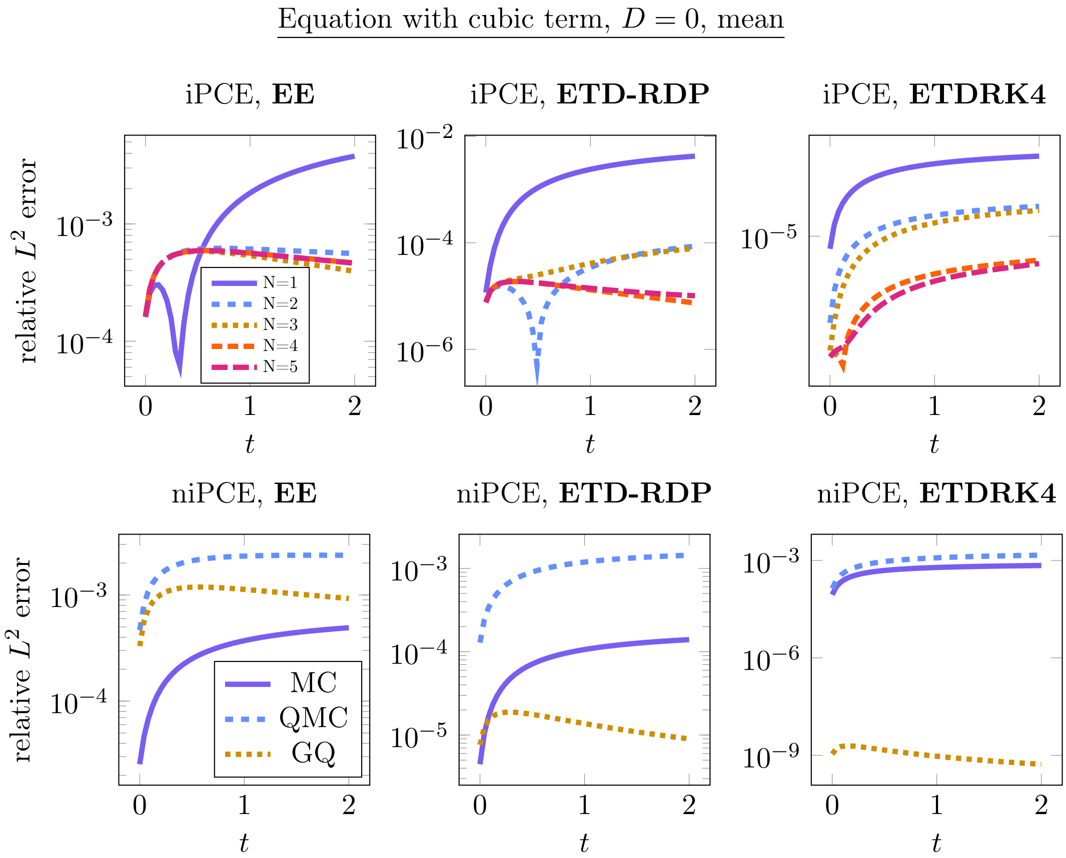

Figure 4.: Plots showing the relative time-dependent error for iPCE schemes (Algorithms 3.5, 3.6, 3.8;, left-hand side) and niPCE schemes (right-hand side) for equation (26) with cubic term ($\kappa = 3$) with diffusion constant $D = 0$.

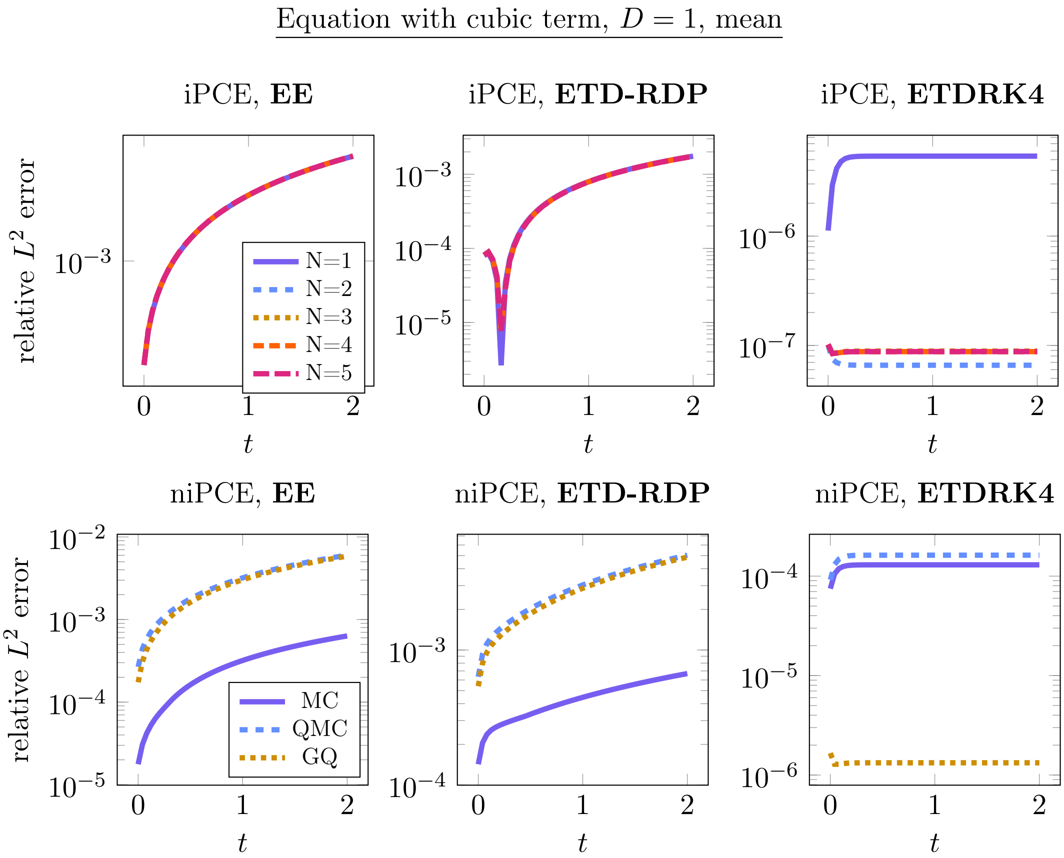

Figure 5.: Plots showing the relative time-dependent error for iPCE schemes (Algorithms 3.5, 3.6, 3.8; left-hand side) and niPCE schemes (right-hand side) for equation (26) with cubic term ($\kappa = 3$) with diffusion constant $D = 1$.

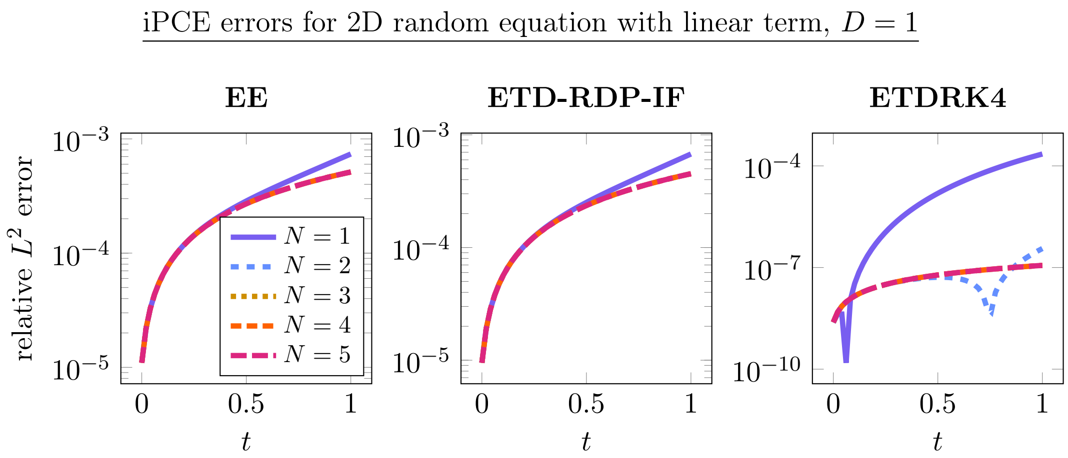

Figure 6.: Time-dependent L^2 errors for equation (30), using the iPCE algorithms 3.5, 3.7, 3.8;. We used the same parameters and numbers of time steps as in the 1D case from Figure 2 in the paper (for the exact parameters, we also refer to Table 3). The exact expected value is given by equation (31). The spatial resolution in the ETD-RDP case was picked in this simulation as $p = 512$. For lower p, the error caused by the finite difference discretization dominates and the curves for different N are identical.

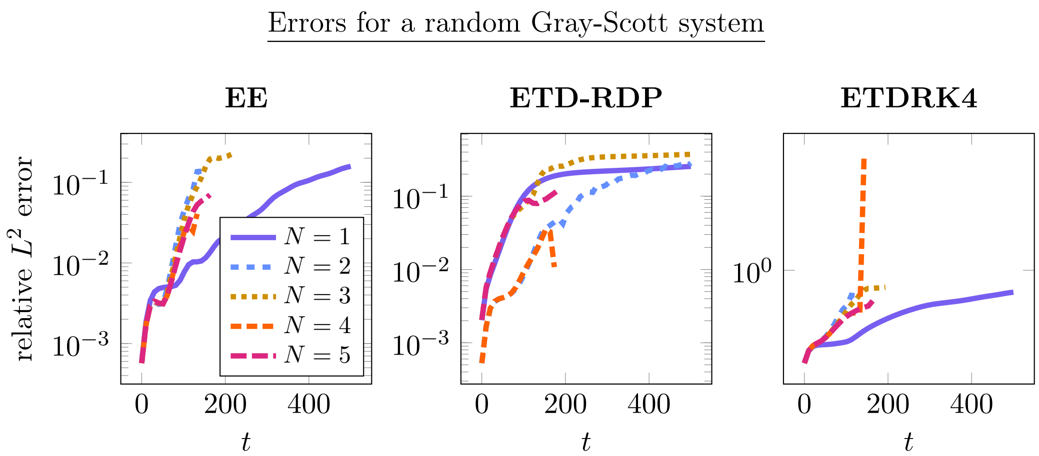

Figure 7.: Time-dependent error plot for a random 1D Gray-Scott system. None of the iPCE schemes work in this case: Initially, the solution is relatively accurate, but as pattern formation starts to occur, iPCE breaks down. For a visual example in two dimensions, see Figure 8.

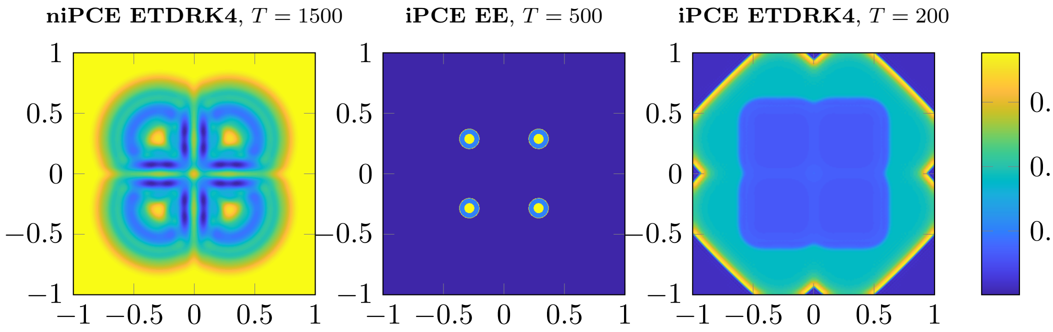

Figure 8.: Simulations for $\mathbb{E}[u(x, T, \cdot)]$ of the random Gray-Scott system (32) with $F = 0.04$ and $k(\omega) \sim \mathcal{U}[0.058, 0.062]$. A niPCE simulation with ETDRK4 (left-hand side) and GQ gives an impression of superimposed patterns for different k. Over time, the four off-center bumps of the initial condition (33) expand and connect, forming intricate patterns as observed on the left-hand side. The EE iPCE simulation fails to correctly propagate the patterns, and the four rings from the initial condition stop expanding. For the ETDRK4 iPCE simulation, the edges of the rings propagate too fast, and no pattern formation is observed.

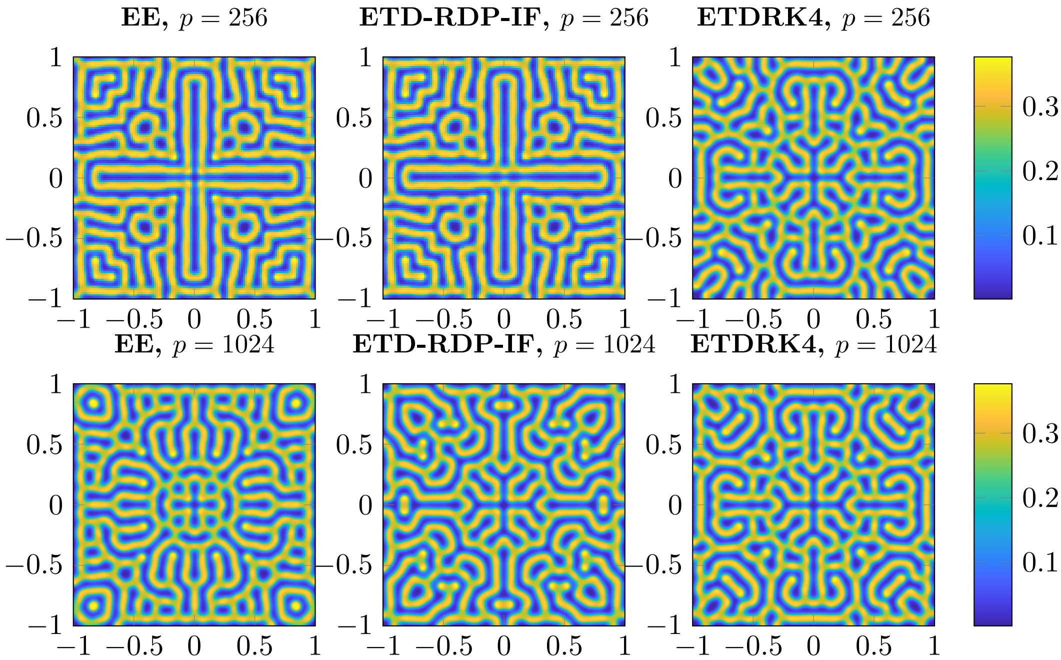

Figure 9.: Deterministic simulations of Gray-Scott patterns for different schemes and resolutions for the same initial condition at $T = 5000$ (using Algorithms 3.1, 3.3, 3.4) . It becomes apparent that after a long-term integration, Gray-Scott patterns are extremely sensitive to the spatial resolution (and number of time steps), and for the correct solution, a high spatial resolution is needed, along with a scheme such as ETDRK4 which performs a spectral approximation in space. The numbers of time steps used are $M = 100000$ for EE and $M = 10000$ for ETD-RDP-IF and ETDRK4.

$D = 0$, linear		
	Intrusive	Non-Intrusive
EE	0.3225	0.6717
ETD-RDP	0.4112	0.2256
ETDRK4	0.4322	0.4244

$D = 1$, linear		
	Intrusive	Non-Intrusive
EE	0.4386	6.4825
ETD-RDP	0.2741	0.3698
ETDRK4	0.7304	0.4809

$D = 0$, quadratic		
	Intrusive	Non-Intrusive
EE	0.5090	0.7563
ETD-RDP	0.3143	0.2550
ETDRK4	0.7242	0.6093

$D = 1$, quadratic		
	Intrusive	Non-Intrusive
EE	3.5583	5.8424
ETD-RDP	0.4906	0.3265
ETDRK4	1.1047	0.4916

$D = 0$, cubic		
	Intrusive	Non-Intrusive
EE	12.6065	0.4934
ETD-RDP	5.2208	0.4339
ETDRK4	6.1375	0.5221

$D = 1$, cubic		
	Intrusive	Non-Intrusive
EE	247.6447	0.3319
ETD-RDP	9.8553	0.5722
ETDRK4	12.4297	0.5626

Table 2.: Runtimes for the created plots, all times in seconds, for iPCE with $N = 5$ and for niPCE with 50 realizations

$D = 0$, linear	iPCE	niPCE	
	M	M	q
EE	1000	2000	50
ETD-RDP	200	200	50
ETDRK4	100	100	50
ETDRK4 ref.		-	-

$D = 1$, linear	iPCE	niPCE	
	M	M	q
EE	20000	20000	50
ETD-RDP	400	200	50
ETDRK4	200	100	50
ETDRK4 ref.		1000	200

$D = 0$, quadratic	iPCE	niPCE	
	M	M	q
EE	1000	2000	50
ETD-RDP	200	200	50
ETDRK4	100	100	50
ETDRK4 ref.		1000	200

$D = 1$, quadratic	iPCE	niPCE	
	M	M	q
EE	10000	20000	50
ETD-RDP	400	200	50
ETDRK4	200	100	50
ETDRK4 ref.		1000	200

$D = 0$, cubic	iPCE	niPCE	
	M	M	q
EE	1000	500	50
ETD-RDP	200	200	50
ETDRK4	100	100	50
ETDRK4 ref.		1000	200

$D = 1$, cubic	iPCE	niPCE	
	M	M	q
EE	20000	20000	50
ETD-RDP	400	200	50
ETDRK4	200	100	50
ETDRK4 ref.		1000	200

Table 3.: Numbers of step sizes M and of samples (for niPCE) for each simulation shown in the paper. 'ETDRK4 ref.' refers to the reference solution used for that simulation. For the linear equation with $D = 0$, the exact solution is known.